

c.2



Lawrence Berkeley Laboratory

UNIVERSITY OF CALIFORNIA

Materials & Molecular Research Division

EROSION-CORROSION-WEAR PROGRAM

Alan V. Levy

July 1980

RECEIVED
LAWRENCE
BERKELEY LABORATORY
AUG 21 1980
LIBRARY AND
DOCUMENTS SECTION

TWO-WEEK LOAN COPY

This is a Library Circulating Copy
which may be borrowed for two weeks.
For a personal retention copy, call
Tech. Info. Division, Ext. 6782



LBL-11109
c.2

DISCLAIMER

This document was prepared as an account of work sponsored by the United States Government. While this document is believed to contain correct information, neither the United States Government nor any agency thereof, nor the Regents of the University of California, nor any of their employees, makes any warranty, express or implied, or assumes any legal responsibility for the accuracy, completeness, or usefulness of any information, apparatus, product, or process disclosed, or represents that its use would not infringe privately owned rights. Reference herein to any specific commercial product, process, or service by its trade name, trademark, manufacturer, or otherwise, does not necessarily constitute or imply its endorsement, recommendation, or favoring by the United States Government or any agency thereof, or the Regents of the University of California. The views and opinions of authors expressed herein do not necessarily state or reflect those of the United States Government or any agency thereof or the Regents of the University of California.

LBL-11109

EROSION-CORROSION-WEAR PROGRAM

Alan V. Levy

Materials and Molecular Research Division
Lawrence Berkeley Laboratory
University of California
Berkeley, California 94720

Excerpt from LBL-10000

Prepared for the U.S. Department of Energy under Contract W-7405-ENG-48.



Lawrence Berkeley Laboratory

University of California
Berkeley, California 94720
Telephone 415/486-4000
FTS: 451-4000

Materials and Molecular Research Division
Building 62 - Room 351 - Phone: 486-5822

July 1, 1980

Dear Colleague:

Another year has passed and the graduate students and post-doctoral fellows in my group at the Lawrence Berkeley Laboratory have continued their research projects in the erosion/corrosion field. As I did last year, I am sending you a summary of our work in 1979. The summaries were originally prepared for our Division's annual report and, hence, are in 2-column format. An LBL report has been published on each subject presented in the summary and is available to you upon request. I hope that the summary and the reports will be of some value to you in your work.

The equipment upon which the experimental work was done is available to you for the generation of data to satisfy your individual needs. Several research organizations have already taken the opportunity to send their researchers to Berkeley to generate erosion data. Please feel free to join them. The only costs are for the consumable materials you or your people will use. Scheduling of outside and graduate student work has been no problem thus far.

Thank you for your continuing interest in our program.

Sincerely yours,

Alan V. Levy
Research Group Manager
(415) 486-5822

AVL/vk

Enclosure

4. Engineering Materials

a. Erosion-Corrosion-wear Program*

Alan V. Levy, Investigator

Introduction. Erosion-corrosion studies have been conducted to gain a fundamental understanding of the mechanisms that are active when small particles entrained in gas or liquid carrier fluids impact the containment wall surfaces of coal conversion system components. Considerable advancements have been made in defining the mechanical and metallurgical interrelationship between an impacting particle and the surface which it impacts upon. A documented mechanism of material loss has been identified that markedly changes the basis for developing models for erosion loss in ductile materials. The forces transferred into a target material by a single impacting particle 600 μm in diameter have been measured.

The fluid mechanics of two-phase flow at low velocities has been defined in a manner that accounts for the aerodynamic contribution of the impacting particle's behavior to the erosion mechanism. By so doing it is now possible to account for experimentally determined velocity exponents in the erosion model up to values of 4, an impossibility heretofore. Also, the pattern of particle distribution in a three-dimensional curved pipe has been analytically established. A laser doppler velocimeter test apparatus is now in place to experimentally verify analytically determined two-phase flow behavior. The erosion behavior of thin scales formed on corrosion resistant stainless steels in elevated temperature oxidizing and sulfidizing gas systems has been determined to be morphology sensitive. An improved design for an elevated temperature, reactive gas erosion tester that can precisely control test conditions has been completed.

The effect of variations in brittle materials, both eroding particles and target surface material, has been investigated analytically and experimentally. The effect of brittle eroding particles of varying hardness and friability of six different minerals on the erosion of ductile aluminum and steel materials has been determined. The experimentally determined behavior patterns have been found to correlate well with the proposed basic mechanism of ductile metal erosion. The erosion of brittle materials as a function of stress and strain patterns in the region of particle impact has been analytically described.

The mechanism of corrosion of stainless steel

in contact with char particles has been determined for a number of environmental conditions of char composition variation and covering bulk gas composition and flow. It has been determined that the char can act as both a source for corroding species and a barrier against their reaching the metal surface from corrosive bulk gases. The behavior of the char as a barrier is more a function of its composition than its depth over the metal's surface.

The principals and diagnostic tools used to study elevated temperature oxidation-sulfidation behavior of metals in coal and oil shale conversion environments have been successfully used to observe surface and bulk characteristics of metal-alumina heterogeneous catalyst pellets and to potentially account for at least some of their change in activity as a function of their service in coal conversion system applications.

Erosion Behavior

1. EROSION MECHANISMS IN DUCTILE METALS[†]

R. Bellman, Jr.

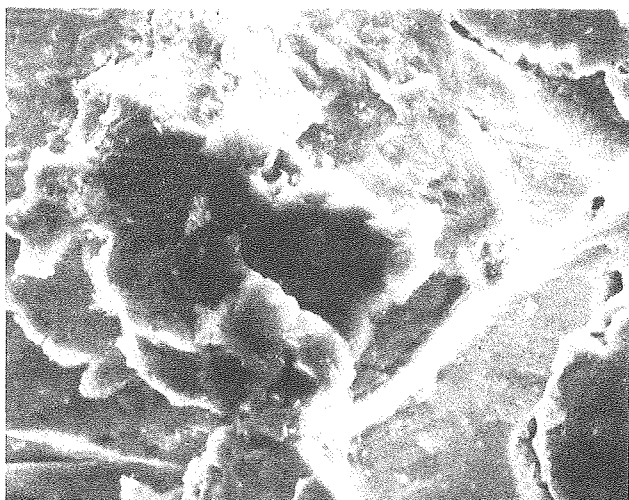
The mechanical mechanism of erosion of a ductile metal by impacting particles has been variously described as a micro machining action¹ or a ploughing behavior² or a brinnelling type of indentation deformation. These mechanisms have been used to establish analytical models, none of which completely defines the behavior. In order to establish a better foundation for modelling, an experimental technique has been developed that meticulously observes sequential deformation of metal surfaces, a particle impact at a time, using the SEM and considerable patience. By following the behavior of a specific area under the SEM from the beginning of erosion deformation of the surface to steady state erosion, a single, pervading mechanism has been documented that occurs at shallow and steep impingement angles alike. This mechanism is a smearing of surface material by a combined forging-extrusion of the surface that produces small platelets that are eventually knocked off the surface by succeeding particle impacts. No cutting action that would create fresh surface in the bottom of an impact formed crater was observed.

The platelet forming mechanism was observed at impingement angles of 30° and 90° on 1100-0 and 7075-T6 aluminum impacted by 600 μm SiC particles at 100 fps and on 1020 steel eroded at an angle of 30° by 250 μm SiC particles at 100 fps. SEM

* This work was supported by the Division of Materials Sciences, Office of Basic Energy Sciences, U. S. Department of Energy.

observations were made of single impacts on fresh and on steady state eroded surfaces and, sequentially, of surfaces impacted by 0.1, 0.2, 0.3, 0.4 and up to 2 gm of particles. Platelet formation is accompanied by localized adiabatic heating of the immediate area affected by the particle's impacting force to temperatures of the order of the annealing temperature in the case of the aluminum.³ The heating results in little difference in the appearance of the impacted area between soft, 1100-0 aluminum and the much harder 7075-T6 aluminum alloy. Cold working of the surface by the deformation from particle impacts does appear to occur below the surface smeared material, resulting in platelets being formed and broken off more readily as erosion continues, but no basic change in the smearing, platelet forming mechanism.

Figure 1 shows an area on the surface of a steady state eroded 7075-T6 aluminum specimen that was subsequently eroded with an additional 1 and 2 gm of particles. The deformed platelets on the surface can be seen in the upper photograph, which



20 μ m

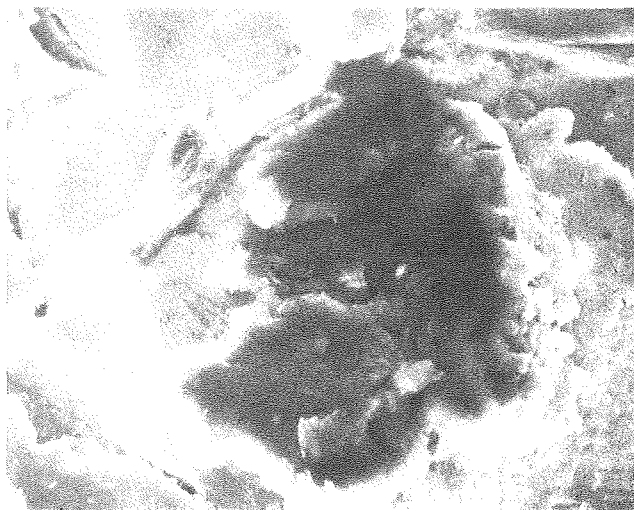
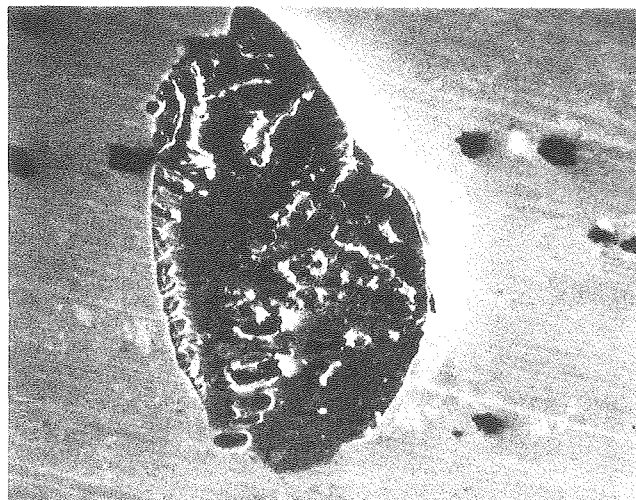


Fig. 1. Sequential removal and formation of platelets in 7075 Al by 600 μ m SiC particles at 100 fps. (XBB 7910-13307)

is of a shallow crater. In the lower photo, after an additional gram of particles had been impacted upon the surface, some of the platelets are shown to have been removed and others formed. The nature of the platelet activity in the area shown is somewhat stylized and represents the mechanism in a simple form. Most material removal observed does not have as ideal a configuration of the platelets. However, essentially no cutting of chips has been observed.

Figure 2 shows a single particle impact crater on a 7075-T6 aluminum surface that was coated with gold before being impacted by a 600 μ m SiC particle at an angle of 30° and velocity of 150 fps. The particles in the unaffected areas of the surface and in the crater are the typical contaminant particles which occur in 7075 alloy. While the impact crater is relatively deep, some of these particles remain in its surface, indicating that the crater was formed by a smearing type rather than a cutting action. An x-ray map of gold was made of the crater area on the SEM and shows the



20 μ m

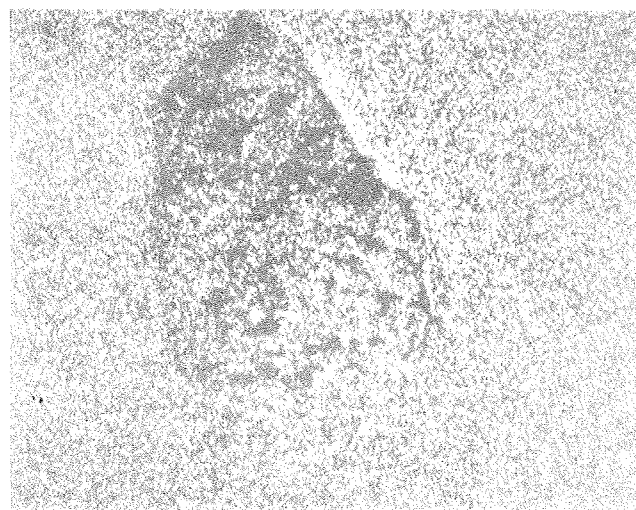


Fig. 2. Single impact crater in 7075 Al surface that was gold coated prior to particle impact. (XBB 7910-13304)

presence of the gold deposited initially on the surface of the alloy across the entire crater surface, a further indication that cutting did not occur in the crater. The buildup of a lip of metal on the right side of the crater is the beginning of the formation of a platelet.

The metallographic observation of the sequential nature of erosion of ductile metals using eroding particle sizes that are representative of those in actual service will be continued to form the basis for an analytical model based upon forging-extrusion mechanisms.

* * *

† Brief version of LBL-10289.

1. I. Finnie, "Erosion of Surfaces by Solid Particles," *WEAR* 3, 87 (1960).
2. J. G. A. Bitter, "A Study of Erosion Phenomena Part I," *WEAR* 6, 5 (1963).
3. R. E. Winter and I. M. Hutchings, "The Role of Adiabatic Shear in Solid Particle Erosion," *WEAR* 34, 141 (1975).

2. EROSION OF THIN SCALES[†]

J. Maasberg

The surface degradation of stainless steels by the combined erosion-corrosion mechanism which occurs at elevated temperatures in coal gasification systems is a function of the formation rate of the protective scales on their surfaces and the removal of those scales by impacting solid particles. An investigation of the erosion behavior of the thin (1-5 μm) Cr_2O_3 barrier scales formed on 310SS in oxidizing and combined oxidizing-sulfidizing gases at 982°C has been carried out by eroding them at room temperature. The erosion behavior of Al_2O_3 barrier scales formed on an experimental Fe-18Cr-5Al-1Hf was also investigated.

Significant differences in the erosion behavior of the scales occurred as the result of variations in the oxygen content of the gas used to develop the scale, the presence of sulfur in the gas, the formation of SiO_2 at the scale-metal interface, and between Cr_2O_3 and Al_2O_3 protective scale compositions. Little difference in the erosion behavior occurred as the result of the surface condition of the alloy prior to scale formation, the temperature of scale formation, preoxidation, the activities of oxygen and sulfur in the gas at levels where sulfide formation did not occur, and the angle of impingement (30° and 90°) of the impacting 50 μm SiC particles at 100 fps velocity.

Figure 1 plots the erosion weight loss vs. amount of eroding particles for 310SS eroded in an air atmosphere ($\text{PO}_2 = 0.2$ atm) and in two low oxygen activity gases ($\text{PO}_2 = 10^{-15}$, 10^{-19} atm) and for a Fe-18Cr-5Al-1Hf alloy. The greater erosion loss for the air oxidized Cr_2O_3 barrier scale of the 310SS compared to the Cr_2O_3 formed in the low oxygen content gases was determined to be primarily due to the presence of internally

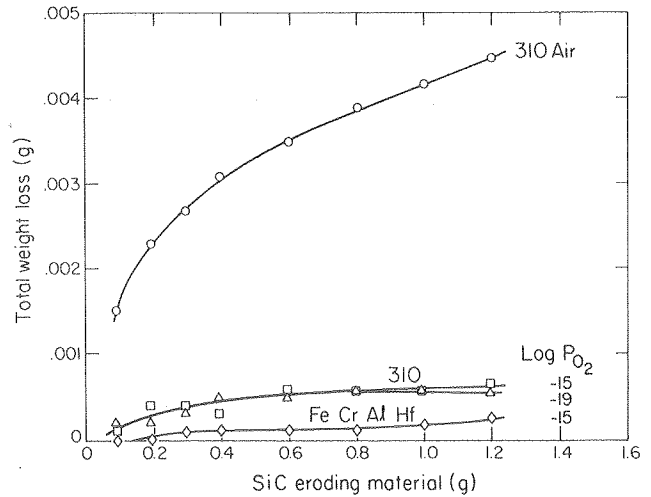


Fig. 1. Erosion of thin scales on 310SS and Fe-18Cr-5Al-1Hf formed at 982°C at different oxygen partial pressures. (XBL 793-803)

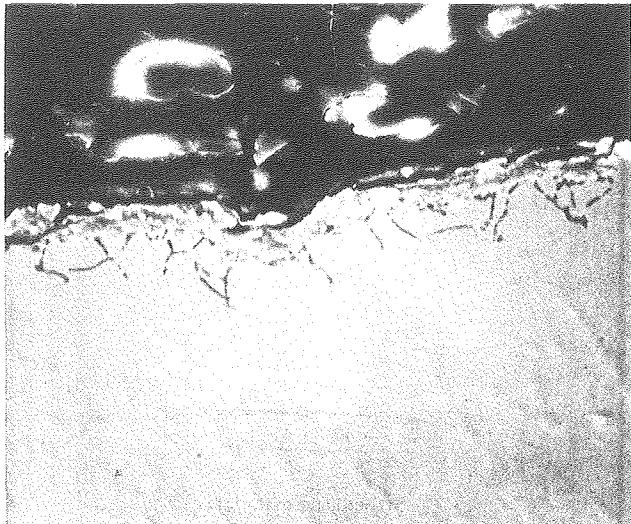
formed SiO_2 at the metal-scale interface. The more continuous SiO_2 layer in the air formed oxide scale and its orientation parallel to the scale-metal interface degraded the bond between the scale and the metal, enhancing its loss by erosion. Less SiO_2 formed in the low PO_2 exposures and no SiO_2 formed in the Al_2O_3 forming alloy, whose scale eroded the least. The presence of small amounts of Si in the 310SS was responsible for the formation of the SiO_2 .

Figure 2 compares 310 stainless steel with the Fe-18Cr-5Al-1Hf alloy. The Fe-Cr-Al-Hf alloy eroded less and this is attributed to the pinning seen in the scale-metal interface as well as the absence of SiO_2 near the scale-metal interface.

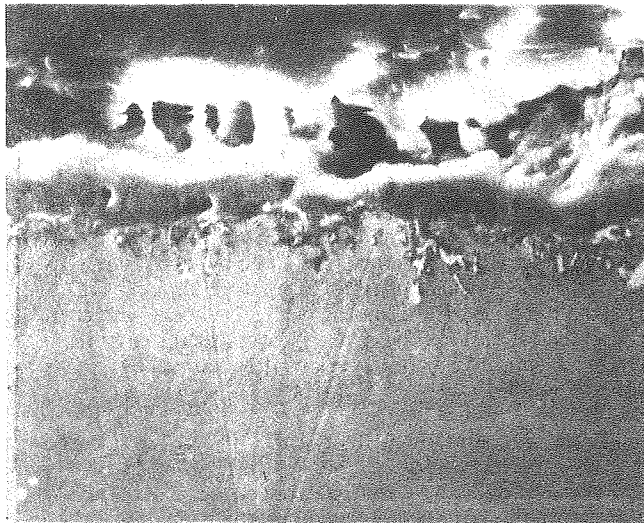
After comparing erosion rates with the morphologies of the scale-metal interfaces, it appears that there are three types of interfaces which can form, each corresponding to a different degree of susceptibility to erosion. Figure 3 shows the types of interfaces. The first type shows a pinning between the outer oxide scale and the metal due to the action of an internally formed oxide. This scale showed the least amount of erosion. The second type shows a smooth contact between the metal and the oxide, with the internally formed oxide having little influence over the erosion. This type of interface showed a moderate amount of erosion. The third type of interface shows an internal oxide running parallel under the surface scale. This type exhibited a high degree of erosion due to a lack of bonding between the metal and the scale.

* * *

† Brief version of "Erosion of Oxide Scales on Metal Substrates," Proceedings NACE Conference on Corrosion-Erosion of Coal Conversion System Materials, Berkeley, California, Jan. 24-27, 1979.

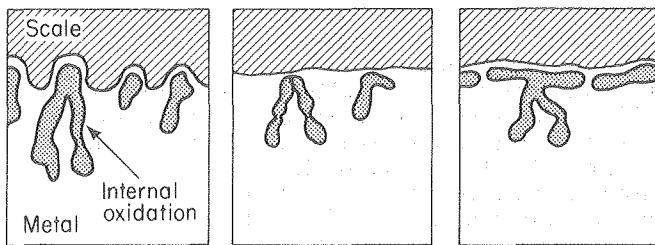


10 μm



5 μm

Fig. 2. Microstructure of 310SS and Fe-18Cr-5Al-1Hf formed at $PO_2 = 10^{-15}$ atmos at $900^\circ C$. (XBB 797-8943)



1. Pinning 2. Smooth contact 3. Parallel subscale
 — Increasing ease of erosion —>

Fig. 3. Sketches of morphologies of internally oxidized SiO_2 in 310SS. (XBL 7912-13356)

3. EROSION MECHANISMS IN BRITTLE SOLIDS

M. Khatibloo

An analytical model for erosion of brittle materials has been developed that agrees more closely with observed brittle material erosion cracking mechanisms than previous models in the literature.^{1,2} It relates the very complex stress and fracture distributions in the contact area of an eroding particle in terms of the target material's properties and the velocity, density and radius of the impacting particles. Because of the low velocity of erosive particle impacts in energy conversion system components, a quasistatic condition is assumed with negligible dynamic effects. Two types of particles were considered in the models, each of which results in a distinctive cone or radial crack formation when it impacts the target surface. The spherical particle induces an elastic response in the eroding material while the angular particle usually causes some plastic flow to occur.

The model considers the point of maximum stress intensity factor, K_I , as being the point where fracture as the result of particle impact will initiate. The stress intensities for positions along the surface of the target material out from the area of contact of the impacting particle were calculated for different crack lengths of small, pre-existing flaws in the brittle material's surface, designated C in Fig. 1. The calculations

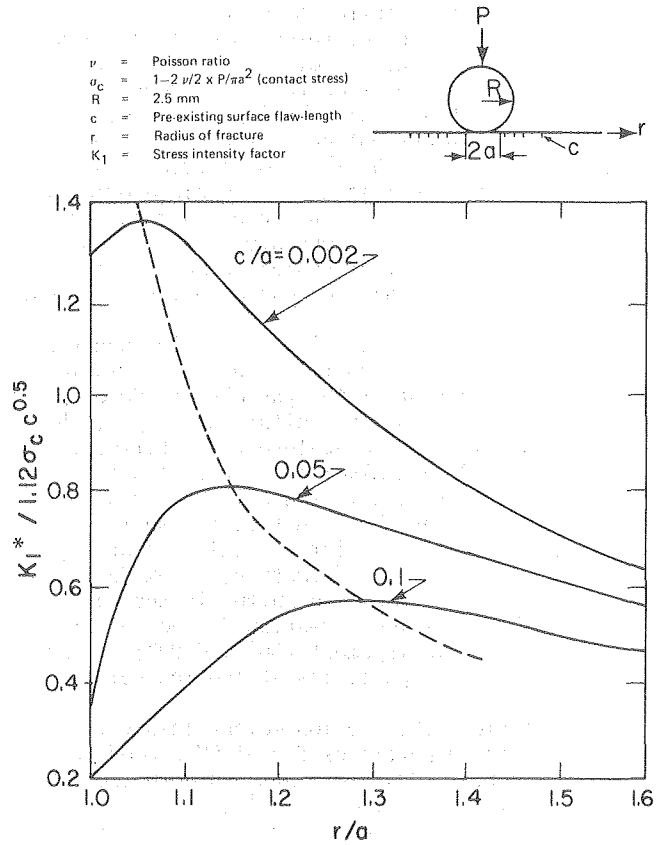


Fig. 1. Variations of the stress intensity factor, K_I^* , with the distance from the contact circle with different surface flaw sizes. (XBL 801-51)

were made for many points out from the particle's area of contact, designated 2a in Fig. 1, along the direction r and plotted, normalizing for the contact area of the particle. It can be seen that as the pre-existing flaw length increases, the normalized stress intensity K_1^* decreases and the position of its maximum out from the area of contact, r , increases (dotted line). Thus, the radius of fracture, r , of the eroding particle impact induced crack changes with the size of the pre-existing flaw. This is shown in Fig. 2. These predicted locations agree with data taken from several literature sources^{3,4} and constitute a major advancement in the development of erosion models for brittle materials.

* * *

1. F. C. Roesler, "Indentation Hardness of Glass as an Energy Scaling Law," Proc. Phys. Soc. B 69, 55 (1956).
2. F. C. Frank and B. R. Lawn, "On the Theory of Hertzian Fracture," Proc. Royal Soc. Series A 299, 291 (1967).
3. H. L. Oh and I. Finnie, "On the Location of Fracture in Brittle Solids," Int. J. of Frac. Mech. 6, 287 (1970).
4. A. S. Argon, Y. Hori, and E. Orowan, "Indentation Strength of Glass," J. Am. Ceram. Soc. 43, 86 (1960).

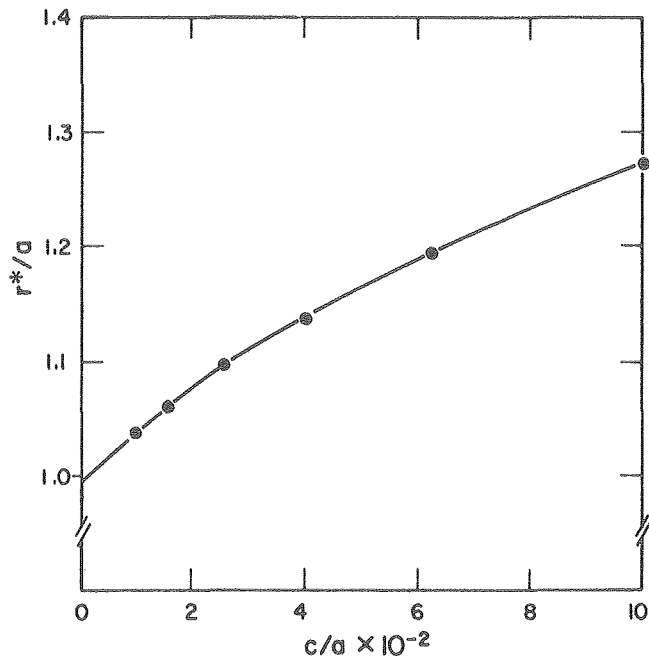
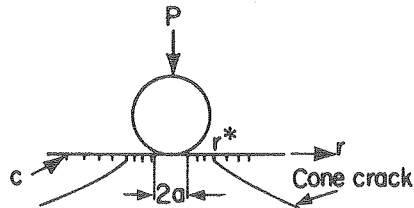


Fig. 2. Variation of the radius of fracture (r) with the surface having pre-existing flaw sizes of length C . (XBL 801-50)

4. EFFECT OF PARTICLE CHARACTERISTICS ON EROSION OF DUCTILE METALS[†]

J. Kim

The effect of the strength, hardness and friability of the impacting particles on the erosion of ductile metals at room temperature has been determined.¹ Most mechanical erosion tests are conducted with particles with Moh hardness greater than 7 and usually 9 or over.² Since char particles in coal gasifiers consist of materials with hardnesses considerably lower than 7, it is important to understand the erosive capabilities of softer particles. Table 1 lists the materials that were tested and the range of hardness they represent. All of the erosion tests were conducted with 50-70 mesh size particles at a velocity of 67 mps (220 fps) at impingement angles of 20° and 90°. The target materials were 1100-0 Al with a VHN = 37 kg/mm² and 1020 steel with a VHN = 194 kg/mm².

Table 1. Impacting particle materials.

Abrasive Particle	MOHS Hardness	Vickers Hardness, VHN (kg/mm ²)
Calcite, CaCO ₃	3	115
Fluorite, CaF ₂	4	180
Apatite, Ca ₅ (PO ₄) ₃ (OH,F,Cl)	5	300
Sand, SiO ₂	~ 7	700
Alumina, Al ₂ O ₃	9	1900
Silicon Carbide, SiC	> 9	3000

It was determined that the nature of the abrasive particle has a significant effect on the erosion of the target materials, particularly in the lower hardness range of the particles. Figure 1 plots the erosion rate of the aluminum and steel as a function of eroding particle hardness. The soft particles are more friable than the hard particles and break up more easily upon impact, blunting the portion of them that transmits the eroding force to the target material and decreasing the effective size of the eroding particle mass. The higher hardness particles retain their size and shape better and this results in increased erosion. This increase is more due to the increasing integrity of the impacting particles than to their hardness.

Above a critical hardness, which was determined to be approximately VHN = 700 kg/mm, the mass and shape of the particles is adequate to have a maximum effect on the target material and further increases in particle hardness had little or no further effect on the erosion rate of the aluminum and steel. The peak in the erosion rate of the aluminum at a VHN = 400 kg/mm relates to the degree of secondary erosion from fragments of the initial particles and the degree of work hardening of the

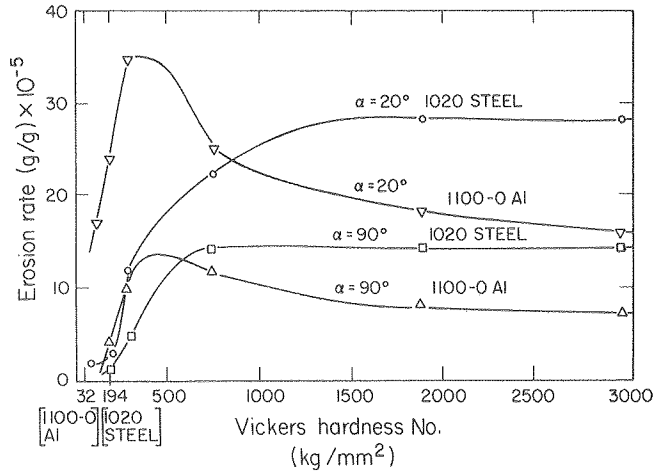


Fig. 1. Effect of impacting particle hardness on erosion behavior of 1100-OAl and 1020 carbon steel at impingement angles, α , of 20° and 90°.

(XBL 801-47)

subsurface area that is caused by the impacting particles and the resultant size of the eroding platelets that can be formed. The shape of the steel curve conforms to Tillys³ curve of particle size vs. erosion rate, further indicating that the size of the effective eroding particle is determining the erosion rate and not its hardness.

* * *

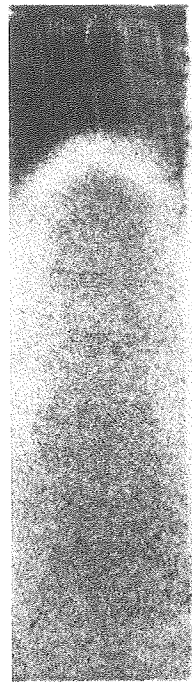
†Brief version of LBL-10268.

1. K. Nellinger and H. Uetz, *Wear* **1**, 225 (1954).
2. Iain Finnie, *Wear* **19**, 81 (1972).
3. J. Goodwin, W. Sage, and G. Tilly, "Study of Erosion by Solid Particles," *Proceedings of Institution of Mechanical Engineers (London)* vol. 184, 279 (1969).

5. THE HALO EFFECT IN JET IMPINGEMENT SOLID PARTICLE EROSION TESTING OF DUCTILE METALS[†]

L. Lapidés and A. Levy

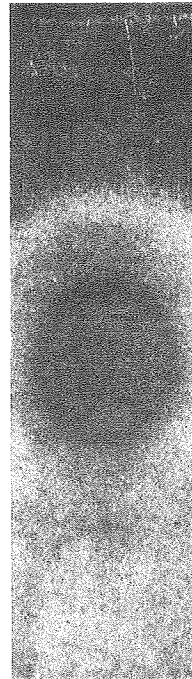
Two different areas of erosion occur on flat test specimens exposed to gas solid particle erosive streams where the stream diameter is smaller than the specimen surface dimensions. The inner area accounts for the majority of the weight loss (see Fig. 1). This area sees the set test conditions of velocity and impingement angle. Erosion also occurs outside this area in an area designated as the "halo area". The weight loss in this area depends on the impingement angle of the particles, and ranges from as high as 25% of the total weight loss at 15° to 3% of the total weight loss at 60°. Figure 2 shows the geometry of the impingement; Table 1 shows the values of the variables. A definite boundary was observed between the two areas. This halo erosion effect was found to be primarily due to the velocity distribution of the particles in a cone around the



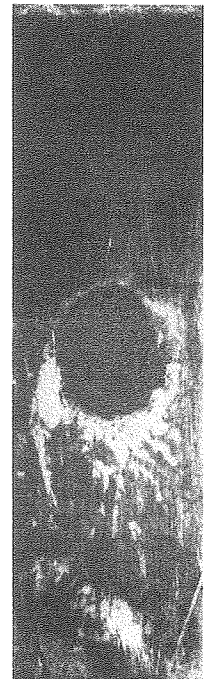
15° Unmasked



15° Masked



60° Unmasked



60° Masked

Fig. 1. Masked and unmasked specimen appearance after erosion at impingement angles of 15° and 60°. (XBB 7810-13575A)

principal column of particles striking the specimen. Table 1 shows that the velocities vary by a factor over 2 between the primary and halo areas. A

Corrosion Behavior

1. CORROSION OF METALS BY CHAR[†]

T. Foerster

The presence of char in coal gasification reactors provides a potential corrodent to metal surfaces that come in contact with it in a static or semi-static mode.^{1,2} A study has been completed to determine the mechanisms of the elevated temperature corrosion that occurs and the effects of variables such as the char composition, quantity of char and bulk gas composition over the char. The 304SS was exposed to the test chars at 982°C for times from 24 to 96 hours.

Figure 1 plots the weight gain of the 304SS for several gas conditions over the char for three different chars; FMC char from W. Kentucky coal, Husky char from North Dakota lignite and Synthane char from Illinois #6 coal. The FMC char was processed at a low temperature in the COED process and retained a significant amount of volatile sulfur while containing a relatively low amount of CaO in its low ash content. The Husky and Synthane chars were processed at higher temperatures which eliminate volatile sulfur from their chars and they contained high quantities of CaO in higher total ash contents compared to the FMC char. These factors explain the resulting weight gain differences.

In the closed exposure retort test with no circulating bulk gas over the char bed, the volatile sulfur in the FMC char was retained in the char, producing a high sulfur activity at the char-metal interface and a resultant greater degree of sulfidation and resultant weight gain. When the stopcock on the retort was opened, the volatile sulfur could escape from the FMC char and the weight gain was reduced. When a 1% H₂S bearing gas was flushed

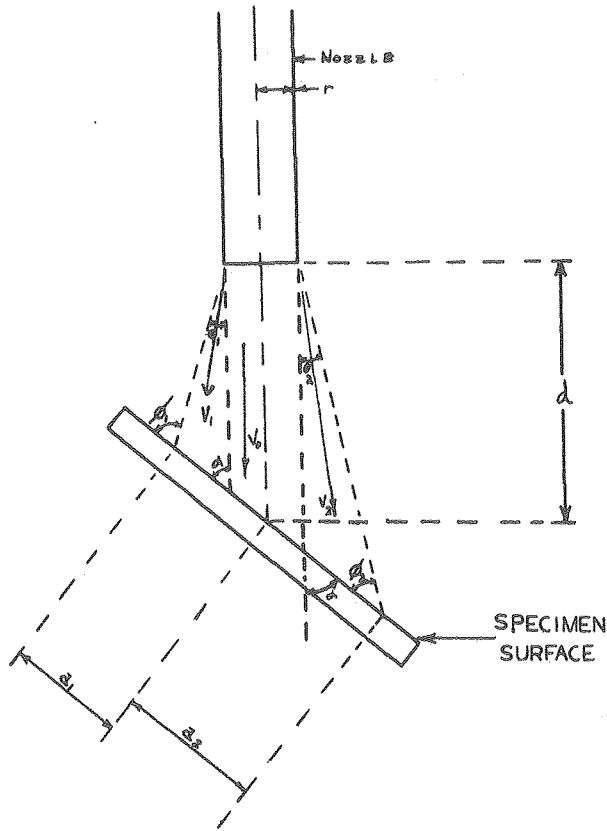


Fig. 2. Diagram of relationship between nozzle and specimen. (XBB 7811-12814A)

Table 1. Values of variables and erosive flow.^a

Area	15°			60°		
	Primary	Boundary	Halo	Primary	Boundary	Halo
Term						
v_1^b	0.15	0.25	0.35	0.15	0.22	0.30
v_2^b	0.75	0.94	1.25	0.17	0.26	0.40
V_1^b	140	123	96	191	126	88
V_2^b	151	134	116	172	117	81
θ_1		4.5°			4.2°	
θ_2		3.4°			5.1°	

^aSee Fig. 2.

^bThese are only relative velocities, not absolute velocities.

secondary effect is the change in the true angle of the particles striking the specimen from the set angle.

* * *

[†]Brief version of LBL-8525.

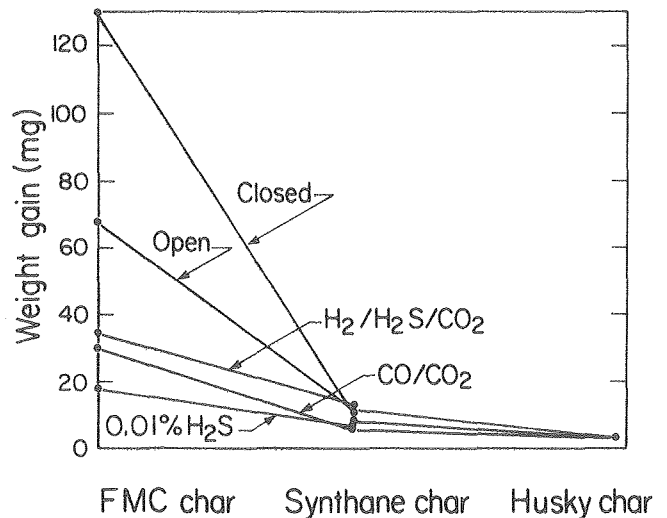


Fig. 1. Weight gain of 304SS exposed to three different chars at several gas conditions. (XBL 795-1670)

through the system, additional volatile sulfur was removed from the FMC char and the weight gain from sulfidation was further reduced, even though the bulk gas had its own sulfur content. When the sulfur activity of the bulk gas was reduced, the bottom two points for the FMC char on the weight gain plot resulted. The Synthane and Husky char specimens had lower weight gains than any of the FMC char specimens because the CaO in those chars acted as a getter for the sulfur that was present. The Husky char had the highest CaO content in its ash of the three chars tested, 13 wt.% composed to 6.5 wt.% for the Synthane char and 4% for the FMC char.

Figure 2 shows the external and internal sulfide scale formed on the 304SS when it was exposed to the FMC char in a closed test retort for 24 hours. Pieces of char were encapsulated in the scale that formed. Figure 3 shows the considerably reduced amount of scale that formed on the 304SS in the test where a 1% H₂S content, moving bulk gas was maintained over the FMC char bed in a 96 hour test.

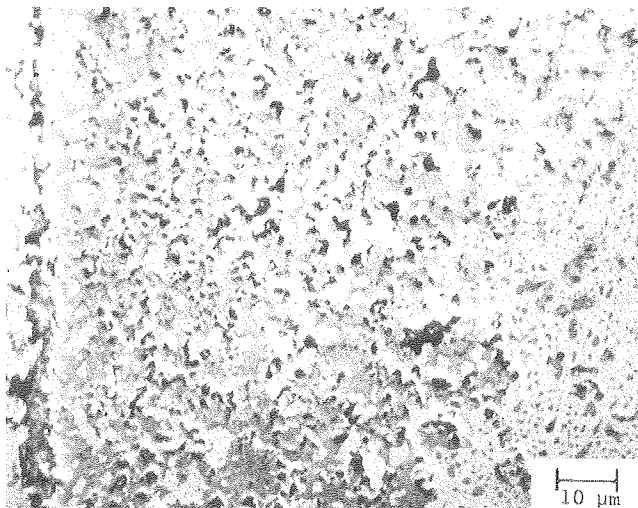
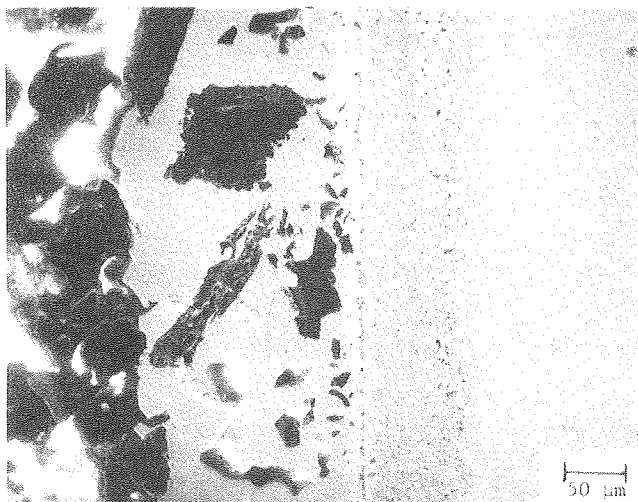


Fig. 2. External and internal sulfide scale formations on 304SS exposed to FMC char in a closed retort for 24 hrs. (XBB 795-6632)

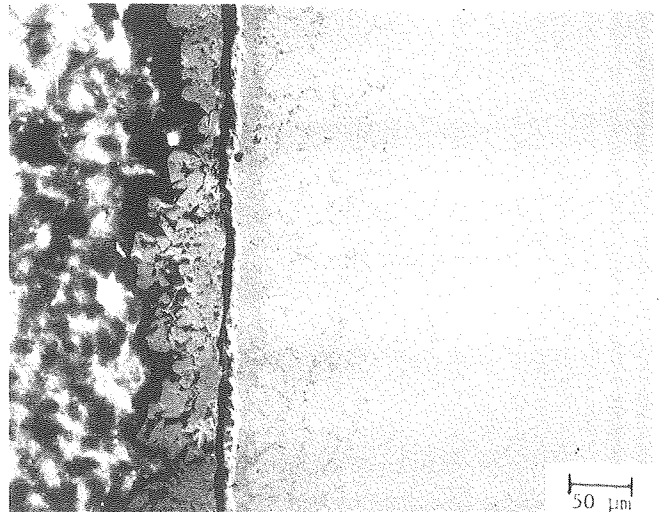


Fig. 3. External and internal sulfide scale formations on 304SS exposed to FMC char with 1% H₂S content flowing bulk gas. (XBB 795-7481)

The increased exposure time resulted in a decreased amount of sulfidation because of the removal of the volatile sulfur from the char by the moving bulk gas.

The Husky and Synthane chars acted as a barrier to the sulfur in the bulk gas, resulting in less sulfidation as the char thickness was increased over the specimens. However, the carbon in the char acted as a getter for the oxygen in the bulk gas and, as the char thickness over the 304SS was increased, the amount of Cr₂O₃ formation on the 304SS decreased.

This project demonstrated the sensitivity of stainless steels to corrosion in contact with chars of varying composition from different gasification processes and starting coals.

* * *

†Brief version of LBL-9308.

1. B. Gordon, "Corrosion of Iron Base Alloys by Coal Char at 871° and 982°C," M.S. thesis, LBL-7604, March 1978.
2. D. Douglass and V. Bhide, "Mechanism of Corrosion of Structural Materials in Coal Gasifier Atmospheres," UCLA, August 1978.

2. CATALYTIC DEACTIVATION[†]

R. Stanley, D. P. Whittle, A. Levy, and H. Heinemann

The use of heterogeneous desulfurization catalysts consisting of silica-alumina supports on which are deposited Ni-Mo, Co-Mo as oxides that could be susceptible to sulfidation in the operating environments of coal conversion systems were studied to determine the nature of the pellet surfaces after service and upon regeneration. Fresh, spent,

and spent and regenerated catalysts of two types were obtained from the Mobil Oil Corp. and metallurgically analyzed. It was determined that relatively thick scales up to 20 μm containing concentrations of sulfur and metallic elements from the environment and from the catalyst pellets formed on the pellet surfaces under some conditions. Surface areas and pore volumes were markedly reduced on those pellets where the scales formed.

Figure 1 shows two cross sections of a pellet of HDS-1441 catalyst that had been used to hydrodesulfurize crude oil. The fresh catalyst shows no scale while the spent and regenerated scale shows a heavy formation of scale. Figure 2 shows the scale highly magnified along with EDAX analyses of its composition at various points. It can be seen that the scale contains concentrations of

sulfur and vanadium, both of which decrease as the analysis moved toward the center of the pellet. The presence of peaks of S, V, Mo, Ti and Fe near the surface of various pellets studied indicates that the metallic constituents of the environment and the catalyst are reacting with sulfur and probably oxygen to form surface scales that can markedly reduce the activity of the catalysts. Concentrations of these elements were verified by electron probe micro analysis. Work is currently underway to use metallurgical techniques to further study surface behavior of desulfurization catalysts.

* * *

† Brief version of LBL-10026

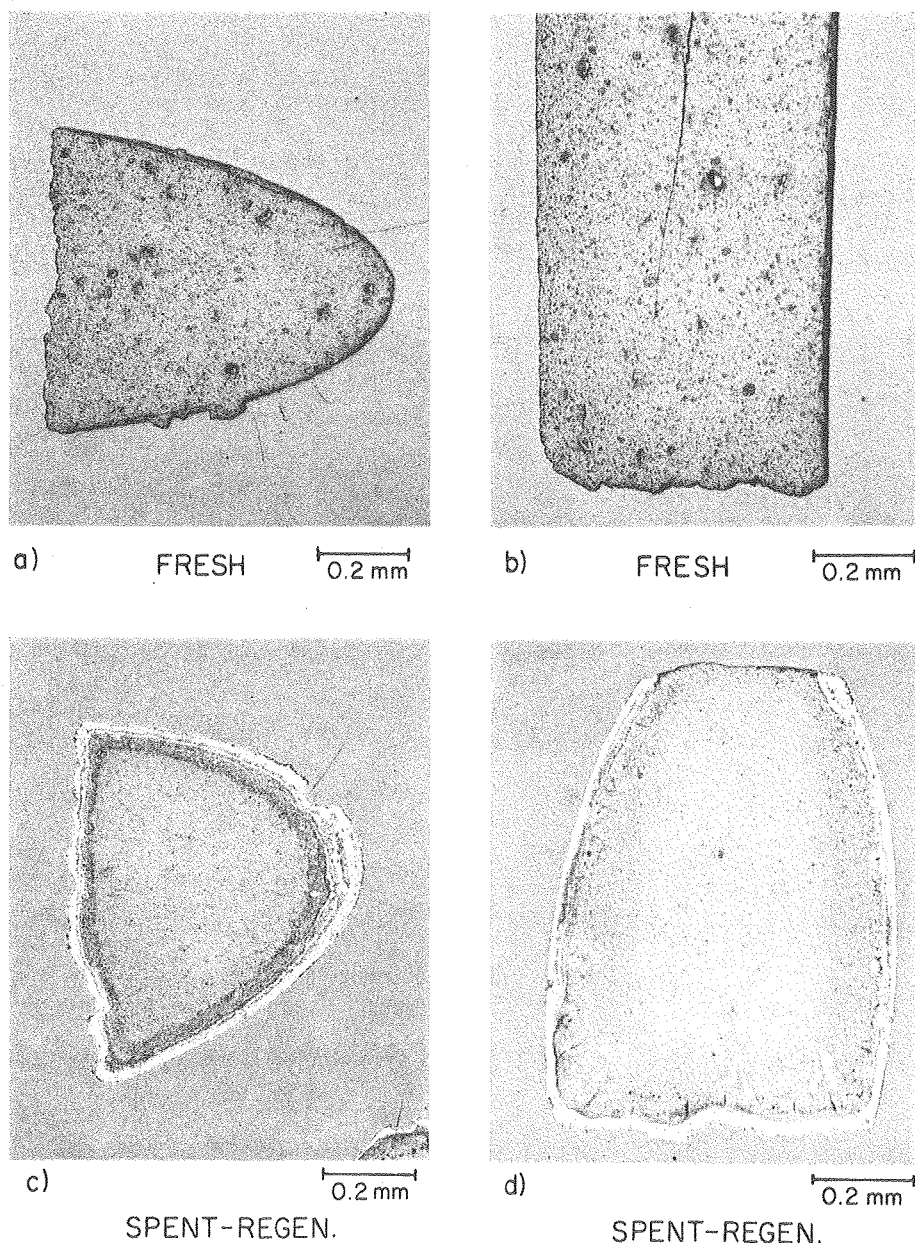


Fig. 1. Scale formation on spent and regenerated desulfurization catalyst pellet. (XBB 802-2169)

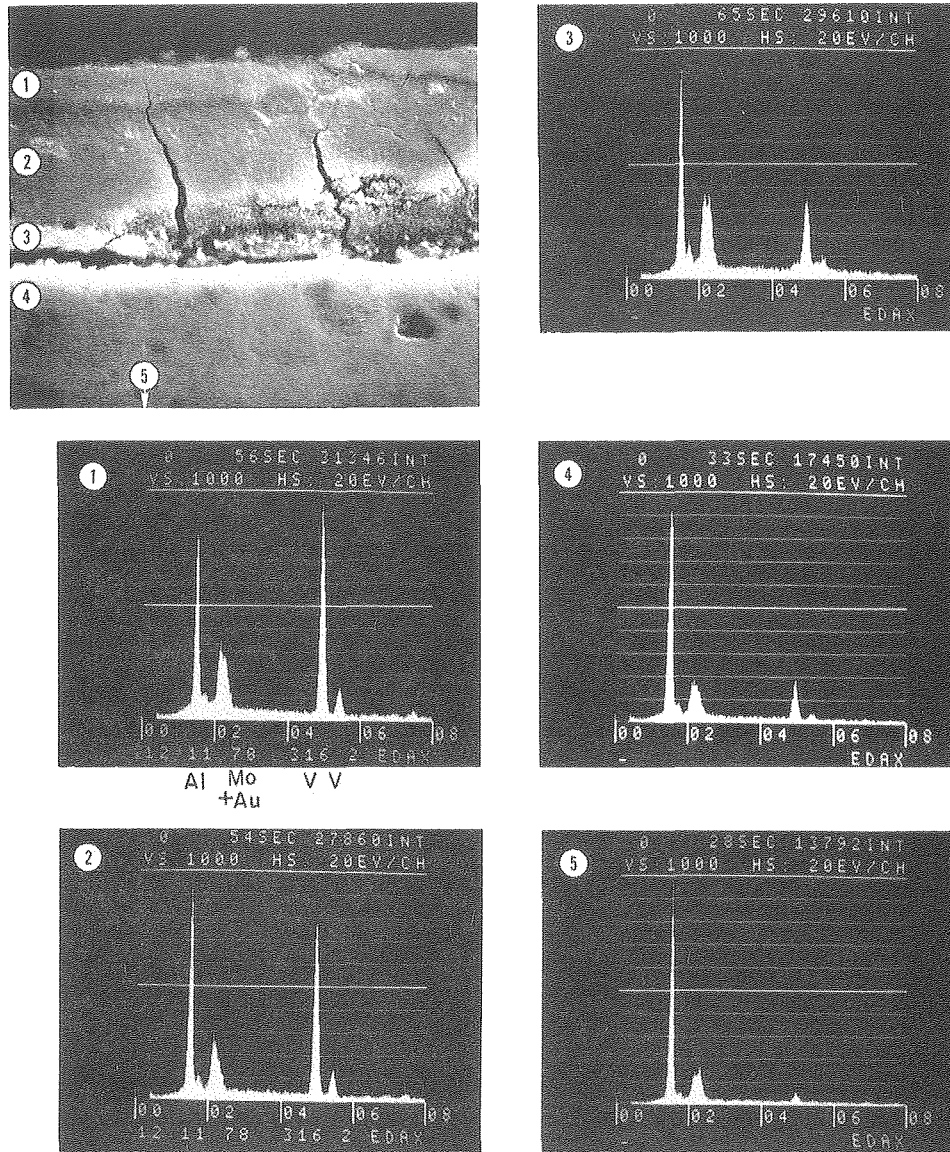


Fig. 2. SEM-EDAX analysis of composition variation of scale formed on desulfurization catalyst pellet. (XBB 802-2167)

Two Phase Flow Behavior

1. GAS-PARTICLE FLOW IN THE ENTRY REGION OF A CURVED PIPE[†]

Woon-Shing Yeung

The fluid dynamics of a dilute gas-particle mixture entering a circular curved pipe has been investigated. The fluid is assumed to be incompressible and the flow nonseparating and laminar. Individual numerical schemes have been devised to handle the two different regions of the fluid flow field, i.e., the irrotational core region and viscous boundary layer region. Thus, in the core region, the traditional Telenin's method is modified to obtain a numerical solution for the velocity potential function. For the viscous boundary

layer, the orthonormal version of the method of integral relations is applied together with a backward difference scheme for the cross derivative terms. Interaction between the two regions is also accounted for by means of a simple iteration scheme.

Since an irrotational core is assumed, the uniform entry profile changes to a two-dimensional potential vortex shortly downstream of the entry section. This is consistent with a recent experimental investigation on entry curved pipe flow by Agrawal, Talbot and Gong.¹ There is also a cross flow directed from the outer bend towards the inner bend in the immediate neighborhood of the entry section. Further downstream, the cross flow reverses its direction and moves from the inner bend towards the outer bend, as is generally

reported in all curved pipe investigations. The axial profile, however, does not change drastically from that of a uniform profile because of the weak interaction between the core and boundary layer region for the values of Reynolds number considered in this report ($Re\ 10^4 \sim 10^5$).

To assess the erosion of the pipe by the particles the dynamic equations of the particle phase are solved. Lagrangian equations of motion for the particle phase are used. Due to the complication of the momentum coupling between the two phases (i.e., the gas phase and the particle phase), only the first order solution for the particle phase has been obtained by neglecting its effect on the gas flow field. This has been proved adequate, for example, in the erosion calculation of a curved pipe carrying a gas-solid mixture. Figure 1 shows particle paths for flow in the

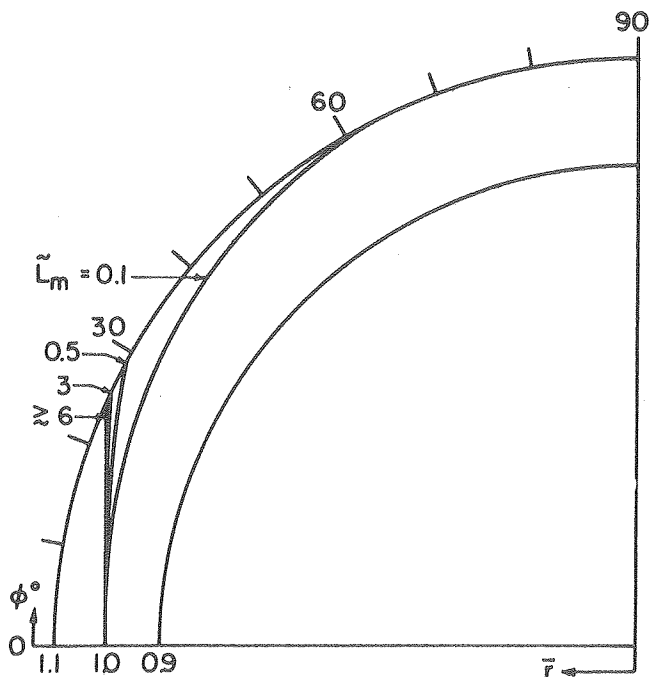


Fig. 1. Particle paths for values of $\tilde{\lambda}_m$, a measure of a particle's momentum. The gas flow is in the direction of ϕ° . \bar{r} is the nondimensional radius of curvature. (XBL 795-6224A)

curved pipe. The impact points indicate the position in the pipe where primary erosion occurs. Primary erosion points are the points at which the particles first strike the wall in the figure.

* * *

† Brief version of LBL-9905.

1. Y. Agrawal, L. Talbot, and K. Gong, *J. Fluid Mech.* 85, part 3 (1978).

2. SEPARATION EFFECTS IN GAS-PARTICLE FLOWS AT HIGH REYNOLDS NUMBERS†

Jonathan A. Laitone

Predicting the fluid mechanical characteristics such as particle trajectories and impact velocities of an eroding gas-solid two-phase flow in a containment vessel is crucial for the successful design and operation of coal gasification systems, coal fired turbines, and other energy conversion systems. The difficulties associated with the analysis of gas-particle flows have precluded general solutions, with most research being applied to simple geometries and often to flow conditions that are not particularly useful.

In the present work a general numerical solution is developed which extends a numerical scheme for gas flow developed by Chorin¹ to a solution suitable for dilute gas-solid particle flows over a much wider range of geometries than previously treated. The method is designed to solve the time dependent equations but may be used in the steady state case as well.

The numerical method is applied to the flow of gas and particles about a cylinder. Previously, gas-particle models have utilized a potential flow approximation for the gas motion. The present method predicts boundary layer growth and separation by introducing viscous effects in the gas flow. Figure 1 indicates the discrepancy between potential theory and the exact viscous case for Reynolds Number, $Re = 1000$. For values of λ (a measure of a particles' momentum) less than two, a cylinder placed in the flow is predicted by the viscous effects model to collect less particles than that predicted by potential theory. This is due to the effect of a viscous boundary layer which acts to deflect gas and particles away from the cylinder.

The method also predicts particle motion in the wake region. In Fig. 2 particles of different sizes are entrained in the Karman vortex street and ex-

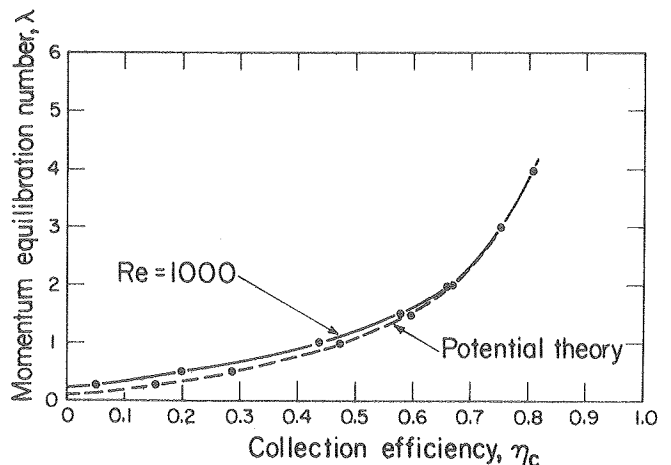


Fig. 1. Particle momentum equilibration number, λ , versus collection efficiency η_c for a cylinder placed in a two phase flow regime. (XBL 799-2769)

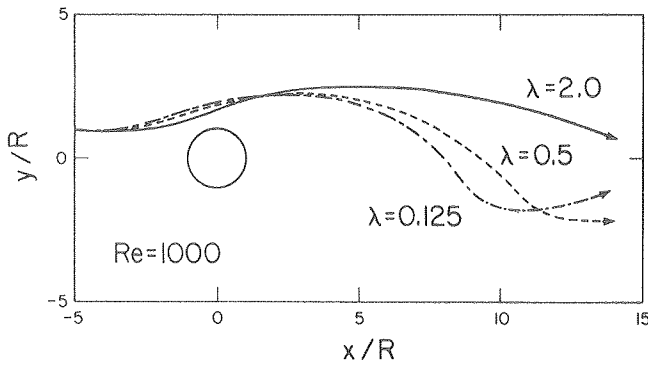


Fig. 2. Trajectories of particles of different particle momentum, λ , over a cylinder of radius R with spatial coordinates of x and y . (XBL 799-2775)

hibit sinusoidal trajectories. Good agreement is found between the numerical results² and experiment.³

* * *

[†]Brief version of LBL-9996.

1. A. J. Chorin, *J. Fluid Mech.* **57**, 758 (1973).
2. J. A. Laitone, *Separation Effects in Gas-Particle Flows at High Reynolds Numbers*, LBL-9996 (1979).
3. G. Grant and W. Tabakoff, *J. of Aircraft* **12**, (No. 5), 471 (1975).

3. AERODYNAMIC EFFECTS IN THE EROSION PROCESS[†]

J. A. Laitone

Experimental investigations of velocity effects on the erosion of a ductile material by aerodynamically entrained solid particles indicate erosion can vary with velocity raised to an exponent up to the order of four in normal or 90° impacts. For smaller angles of attack, the exponent is less than four but greater than two. Previous quantitative erosion models do not predict these high exponent values. In this study,¹ the two-phase fluid mechanical system is analyzed and an analytical expression is presented that predicts particle impact speeds varying with the fluid free stream speed squared in normal impacts (See Fig. 1).

The aerodynamic effects modify the particles impact kinetic energy by increasing the velocity dependence. Including the aerodynamic effect with an equation of motion type erosion model such as Finnie's² yields erosion rates varying with free stream velocity with exponents between 2 and 4; a result experimentally confirmed.³

This is a critical result for the study of erosion of materials. Researchers have attempted to explain why erosion varies with velocity exponents greater than two by considering only particle-surface interaction. Their results are valid only for particles that are not aerodynamically entrained. Experiments with single particles dropped on a surface are devoid of aerodynamic

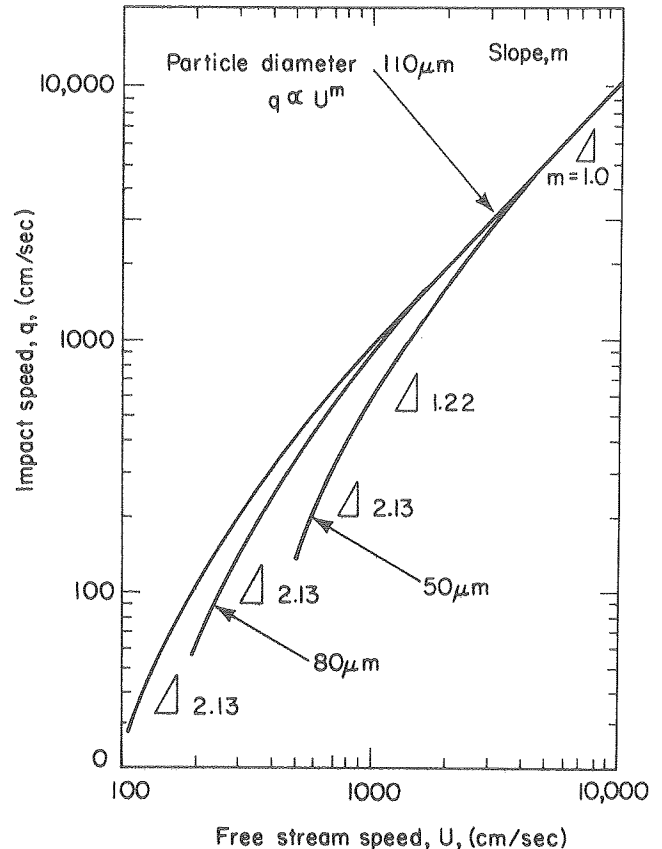


Fig. 1. Effect of free stream velocity on impact speed at the surface. The slope of the curve is given by m . The maximum value of m yields $q \propto U^{2.13}$. (XBL 794-1053)

effects and, thus, the impact speed, q , equals the free stream speed, U , far from the surface. This study indicates the role of aerodynamics in an erosion study. In order to utilize an erosion model in an aerodynamic system, the particle's impact speed which is different from its free stream speed must be used. The impact speed is determined from the free stream speed by solving the fluid mechanical system.

* * *

[†]Brief version of LBL-8962.

1. J. Laitone, *Aerodynamic Effects in the Erosion Process*, Proceedings of the 3rd International Tribology Conference, Paisley, Scotland, Sept. 10-13, 1979.
2. I. Finnie, *Wear* **19**, 81 (1972).
3. G. Grant and W. Tabakoff, *J. Aircr.* **12** (No. 5) 471 (1975).

4. DEVELOPMENT OF A LASER TEST SYSTEM FOR TWO-PHASE FLOW STUDIES

A. Modavi

The major effort over the past three years to analytically describe particle trajectories and

velocities of eroding particles in two phase flows to determine precise particle impacting conditions on target surfaces has developed models for flow over various shaped surfaces. The nature of this flow was used to develop a refined experimental flow system that can test the predictions of the models. Verification of the models will considerably enhance the ability to predict erosion rates of surfaces of different geometries that are containing solid particle-fluid flow systems in coal conversion systems. The test system is particularly designed to be able to produce data that can be scaled to full size component flows. It is unique to the needs of the analytical models developed to describe flow in pipe bends and elbows, in sudden expansions and over sharp corners and about turbine blades, plates and cylinders.

Figure 1 shows the test system. The cold air flow system provides air velocities of 0 to 30 ft/sec up to 0.5 psia differential pressure in 2x2 inch curved rectangular ducting. The test section of the ducting is made of optically clear plastics which allow laser Doppler measurements to be carried out.¹ The Laser Doppler Velocimetry (LDV) is a nonintrusive velocity measurement technique which employs a laser light probe (the intersection of two beams of monochromatic light) to generate a modulated (Doppler shifted) light scattered off various particles' flow through the light probe.² This light scattering is detected by photomultiplier tubes, or other photo detectors, and processed electronically to translate such signals into velocity of the particles.

The diagram at the right side of the figure illustrates a simple LDV system, the actual LDV system employed is a more complex dual color back scattering LDV system. The dual color LDV provides simultaneous measurements of two components of velocity and employs the two primary frequencies of a 2 watt argon ion laser.

A minicomputer is used to provide the record keeping of the particle counts of up to 20 kHz from two Disa LDV processors. The minicomputer also provides the auto-positioning of the LDV optics by commanding a custom made SYZ motorized table to move in 1/1000 mm increments.

The data can be instantaneously processed and displayed/plotted on the computer terminals or can be stored on the magnetic discs for future processing. In addition to the LDV processors a real time signal digitizing capability is available.³

* * *

1. S. Mason and B. Smith, Erosion of Bends by Pneumatically Conveyed Suspensions of Abrasive Particles, Powder Technology, Netherlands, March 1972.
2. F. Durst, et al., Principles and Practice of Laser Doppler Anemometry, Academic Press, San Francisco, California (1976).
3. D. Holve and S. Self, An Optical Particle-Sizing Counter for In-situ Measurements, High Temperature Gas Dynamics Laboratory, Stanford Univ., Stanford, California (1978).

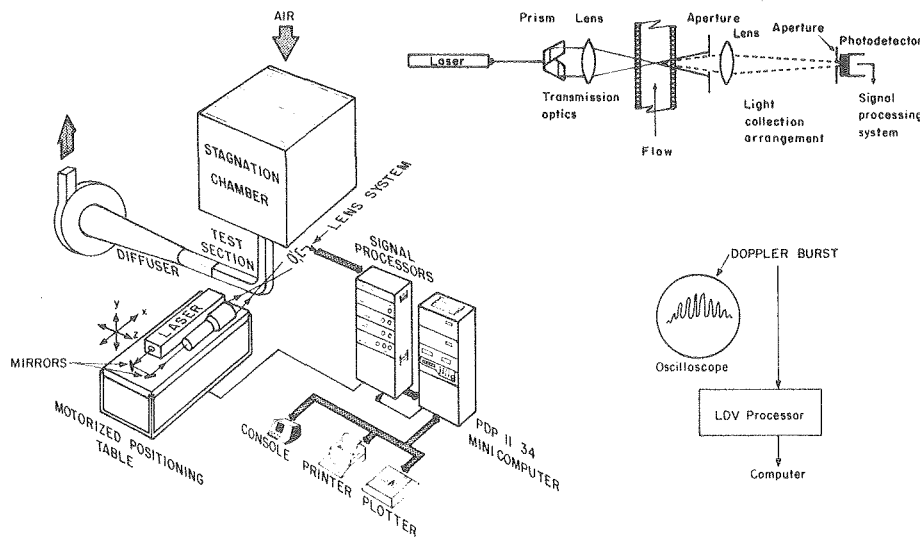


Fig. 1. Schematic of two-phase flow test system and laser Doppler velocimeter. (XBL 801-52)

RESEARCH PLANS FOR CALENDAR YEAR 1980

The mechanism of erosion by the formation of platelets on the surface of a ductile metal will be further experimentally documented and an analytical model will be developed based upon the forging-extrusion mechanism that forms the eroding platelets. Further efforts will be made to define the stresses and strains that occur upon impact of an erosive particle by experimental measurements using the techniques already developed and to utilize them in an analytical model and in defining what properties of a target material enhances erosion resistance. Elevated temperature erosion and combined erosion-corrosion will be studied further.

The effects of coatings of different types and compositions applied by several different mechanisms on the erosion and combined erosion-corrosion behavior of structural metals will be investigated. The combined erosion-corrosion behavior of thin scales on stainless steels will be studied to determine under what environmental conditions each of the mechanisms is governing and how synergistic the combined behavior is.

The fluid mechanics of two phase flow will be studied experimentally to verify model predictions using laser instrumentation. The analytical work will concentrate on adopting initial analytical models to fully turbulent flow conditions. The behavior of two phase flows where the carrier vehicle is a lubricating liquid such as an oil will be analytically described.

1979 PUBLICATIONS AND REPORTS

Refereed Journals

1. J. A. Laitone, "Aerodynamic Effects in the Erosion Process," *Wear* 56, 239-246 (1979), LBL-8962.
2. J. A. Laitone, "Erosion Prediction Near a Stagnation Point Resulting from Aerodynamically Entrained Solid Particles," *J. Aircraft*, AIAA, 16, No. 11 (1979), LBL-6990 Rev.
3. K. Chilquuri, G. Yee, and J. A. C. Humphrey, "Developing Laminar Flow and Heat Transfer in Strongly Curved Ducts of Rectangular Cross Section," *Journal of Heat Transfer* (in press).
4. L. Lapidés and A. Levy, "The Halo Effect in Jet Impingement Solid Particle Erosion Testing of Ductile Metals," *Wear* 58, (1979).
5. B. A. Gordon and V. Nagarajan, "Preliminary Observations of the Thermodynamic Predictions of Fe-Cr-Ni Alloys in Coal Gasifier Environments," *Oxidation of Metals* 13, (No. 2) 197 (April 1979).
6. K. T. Jacob, D. B. Rao, and H. G. Nelson, "Phase Relations in the Fe-Ni-Cr-S System and the Sulfidation of an Austenitic Stainless Steel;" *Oxidation of Metals* 13 (No. 1) 25 (Feb. 1979).

Other Publications

1. A. V. Levy, "Corrosion-Erosion of Materials in Coal Liquefaction Environments," *Proceedings of NACE Conference on Corrosion-Erosion of Coal Conversion System Materials*; p. 174; Berkeley, Calif., Jan 24-26, 1979.
2. G. Zambelli and A. V. Levy, "Erosion of Scales on Metals," *Proceedings of NACE Conference on Corrosion-Erosion of Coal Conversion System Materials*; p. 480; Berkeley, Calif., Jan 24-26, 1979.
3. A. V. Levy and S. Jahamir, "The Role of Plasticity in the Erosion of Ductile Metals," *Proceedings of the 5th International Conference on Erosion by Liquid and Solid Impact*, p. 8-39; Cambridge Univ., England, Sept. 3-6, 1979.
4. G. Zambelli and I. Finnie, "Particulate Erosion of NiO Scales," p. 9-49; Cambridge Univ., England; Sept. 3-6, 1979.

LBL Reports

1. W.-S. Yeung (Ph.D. thesis), "Gas Particle Flow in the Entry Region of a Curved Pipe," LBL-9905.
2. G. Yee and J. A. C. Humphrey, "Developing Flow and Heat Transfer in Strongly Curved Ducts of Rectangular Cross-Section," LBL-9092.
3. J. A. C. Humphrey, J. H. Whitelaw, and G. Yee, "Turbulent Flow in a Square Duct with Strong Curvature," LBL-9650.
4. T. F. H. Foerster (M.S. thesis), "The Effect of Coal Char on the Corrosion of 304SS," LBL-9308.
5. J. A. C. Humphrey, "A Transition State Model for Predicting the Rate of Erosive Wear of Ductile Materials by Solid Particles," LBL-10011.
6. J. Kim (M.S. thesis), "Effect of Particle Characteristics on Erosion of Ductile Metals," LBL-10268.
7. R. Stanley, D. Whittle and A. Levy, "Characterization of the Degradation of Hydrodesulfidizing Catalysts," LBL-10026.
8. J. Laitone (Ph.D. thesis), "Separation Effects in Gas Particle Flows at High Reynolds Numbers," LBL-9996.

Presentations

1. A. V. Levy, "Role of Plasticity in Erosion," Naval Postgraduate School, February 1979.
2. A. V. Levy, "Erosion of Oxide-Sulfide Scales on Metals," Gordon Research Conference, New London, N.H., July 1979.
3. A. V. Levy, "Erosion Mechanisms in Metals," U. S. Army Research Office Conference; Sanibel Island, Fla., October 1979.

4. J. A. Laitone, "Erosion Prediction Near a Stagnation Point Resulting from Aerodynamically Entrained Solid Particles," Paper No. 79-0555, AIAA 15th Annual Meeting, Washington, D.C., February 1979.

5. J. A. Laitone, "Aerodynamic Effects in the Erosion Process," 4th International Tribology Conference, Paisley, Scotland, September 1979.

6. G. Yee and J. A. C. Humphrey, "Developing Laminar Flow and Heat Transfer in Strongly Curved Ducts of Rectangular Cross Section," Paper No. 79-WA/HT 15, ASME Winter Annual Meeting, Heat Transfer Div., New York, N.Y., December 1979.

c. Coal Liquefaction Alloys Test Program*

Alan V. Levy, Investigator

Introduction. The behavior of ductile metals in both cast and wrought forms in the erosion-corrosion environments that occur in coal liquefaction process components from the actions of elevated temperature coal-solvent slurries are being studied. New information is being developed on the role of such variables in the slurry as solids content, velocity, entrained moisture and gas content, viscosity, temperature and particle comminution in promoting or retarding erosion behavior of metal alloys. Different alloys have opposite rankings of erosion resistance in different slurries with relatively small differences in the slurry. Distinct geometry effects on erosion of pipe elbows have been found that vary with slurry velocity and solids loading. Non-dimensional correlation analyses of erosion data have related slurry and target material properties with respect to erosion behavior.

1. EROSION BEHAVIOR OF METALS IN COAL SLURRIES[†]

W. Tsai

The use of the small, two liter capacity slurry pot tester has developed knowledge of the effect of several variables on the erosion of structural metals exposed to non-aqueous coal slurries.¹ Both test conditions and sample composition have been varied. It has been determined that small modifications in test conditions can have major effects on the erosion behavior of different materials.² Comparative erosion rates of A-53 mild steel and 304SS have been reversed by small changes in particle size distribution and initial water content of the coal. Figure 1a shows the erosion of the two steels as a function of drying the coal prior to mixing the slurry. It is probable that a thin film of water formed on at least the larger coal particles, providing an encapsulating energy absorber that markedly decreased the amount of erosion that occurred.

Figure 1b shows that the coal particle solids loading in the slurry has a relatively small effect on the erosion of an A-53 mild steel over the range of coal concentrations typically used in coal liquefaction systems 30-50 wt.%. The effect of velocity difference is significant and can be seen in the curves. Based on the type of data obtained by varying several different test parameters, plots have been prepared giving erosion at known conditions as a function of time. The tangent at time zero to an erosive wear curve is taken as the characteristic rate of erosion in an experiment. This value is correlated, through dimensional analysis consideration with the dimensionless groups characterizing the experiment.

* This work was supported by the Division of Planning and Systems Engineering, Office of Fossil Energy, U. S. Department of Energy.

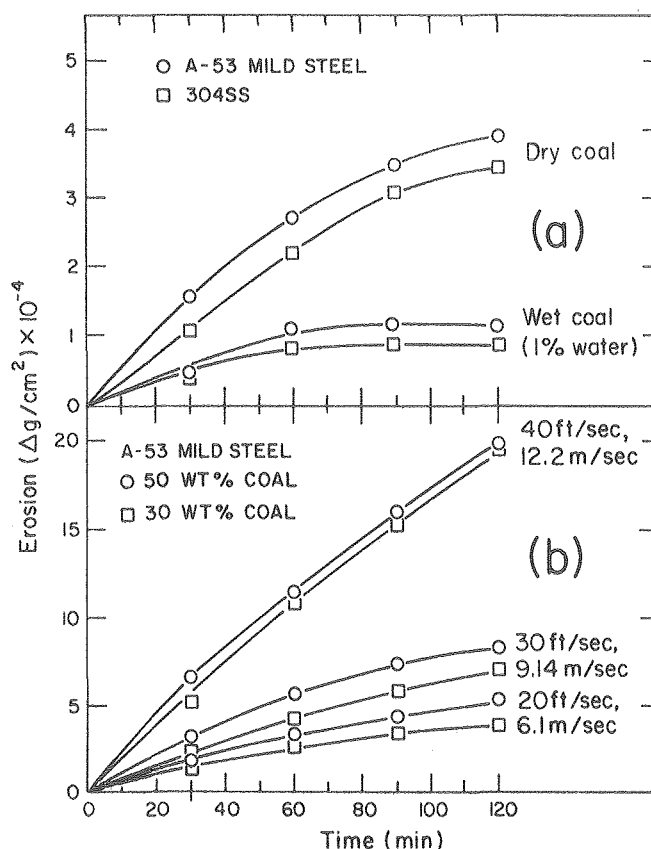


Fig. 1. (a) Effect of water content in 30 wt.% coal on erosion of A-53 mild steel (o) and 304SS (□) in kerosene at 25°C at $V = \text{fps}$. (b) Effect of particle concentration and velocity on erosion of A-53 mild steel in kerosene at 25°C using 50 wt.% coal (o) and 30 wt.% coal (□) slurries.

(XBL 801-49A)

Erosive wear of the metal specimens tested (A-53 mild steel, 304SS and 316SS) with coal and silicon carbide particles in kerosene was found to increase with increasing particle density, concentration, velocity and hardness and with decreasing target metal yield strength or hardness. Figure 2 shows the fit of the regressed equation. Data clustered about 9.5 (for coal) has an average error of 19.4% while that clustered about 7.25 (for SiC) has an average error of 14.3%.

* * *

[†]Brief version of LBL-10044.

1. R. Gardi, B. Ricks, and T. Audl, "Control of Erosion-Corrosion in Slurry Pipelines," 1st International Conference on the Internal and External Protection of Pipes, Sect. G-4, pp. 39-52, Sept. 1979.
2. B. Ellison, "Corrosion-Erosion in Multi-Phase Systems," presented at 70th Annual Meeting AiChE, Nov. 1977.

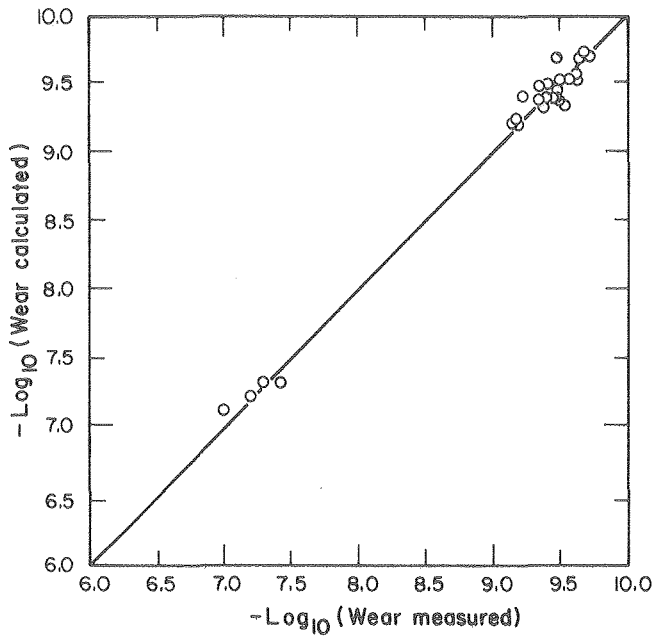


Fig. 2. Comparison of measured and calculated erosive wear. (XBL 801-48)

2. EROSION OF PIPING IN A SLURRY LOOP

A. Shaw and A. Levy

The slurry loop system using a recirculating slurry of 30 and 50 wt% coal in kerosene has been operated in excess of 2000 hrs in a series of tests to determine the erosion behavior of mild steel and stainless steel elbow components at ambient temperature. Figure 1 shows the reduction in piping wall thickness of a side loop to the primary 2" diam. pipe loop. The smaller diameter pipe sections of A-53 mild steel were used to increase the velocity and, hence, the amount of erosion to be able to obtain measurable wall thickness reductions in a reasonable test duration of 250 hours. The numbers opposite each measurement location are the number of thousandths of thickness reduction as measured by an ultrasonic thickness gage. It can be seen that the erosiveness of the slurry flow increased with velocity and as a function of geometry. For example, the erosion in the entry 2" diam elbow of the side loop where the flow velocity was 8-10 fps (points 1, 2, 3) was considerably less than that of the 2" dia elbow at the exit section (points 31, 32, 33) where the flow from the 1" diam pipe (velocity = 35-40 fps) impinged on the 2" diam elbow as from a nozzle.

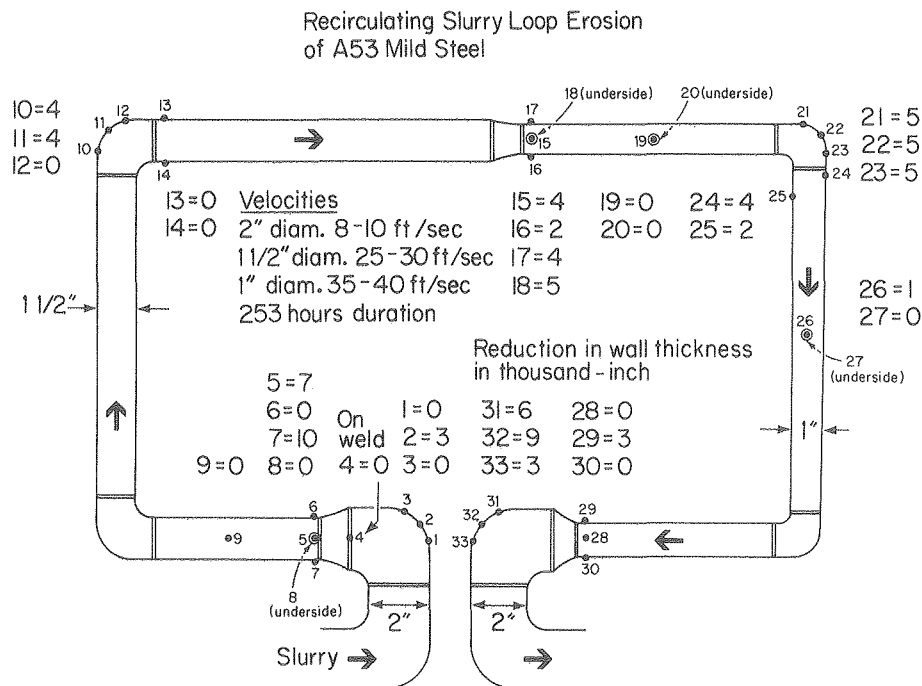


Fig. 1. Erosion thickness loss measurements in a recirculating slurry loop testing A-53 mild steel elbows in a 30 wt.% coal-kerosene slurry. (XBL 7910-4249)

In both elbows maximum erosion occurred at the middle point where the impingement angle was the greatest.

In a subsequent test, 304 and 316SS had comparable thickness reductions. When the slurry viscosity was increased by increasing the wt.% of coal in the kerosene from 30 to 50 wt.%, the amount of erosion for 304 and 316SS was reduced by approximately half.

RESEARCH PLANS FOR CALENDAR YEAR 1980

The erosion behavior of additional materials, including some coatings on mild steel substrates will be determined at several temperatures using a range of slurry variables. The data will be used to further develop the erosion rate prediction model. Extensive use will be made of the jet impingement tester to direct slurries at flat surface specimens of several materials in a once-through mode for the eroding particles. The unit's slurry capacity has been increased by several times to permit longer runs to be made. The slurry loop will continue to operate at ambient and elevated temperatures in a new flow passage design and

using specimens which can be disassembled readily to obtain mechanical thickness measurements of the amount of erosive wear.

1979 PUBLICATIONS AND REPORTS

Other Publications

1. A. V. Levy, I. Cornet, and D. Abdollahnian, (Quarterly Report) January 1979, LBID-020.

LBL Reports

1. W. Tsai, J. A. C. Humphrey, I. Cornet, and A. V. Levy, "Experimental Measurement of Accelerated Erosion in a Slurry Pot Tester," LBL-10044.

Invited Talks

1. A. V. Levy, "Erosion-Corrosion in Coal Liquefaction Systems," Golden Gate Metals and Welding Conference, San Francisco, Calif., Feb. 1979.
2. A. V. Levy, "Coal Liquefaction Alloy Test Program," 3rd Annual Coal Conversion Materials Conference, Gaithersburg, MD, Oct. 1979.

d. Oil Shale Retort Components*

A. Levy and D. Whittle, Investigators

Introduction. The corrosion of alloy and stainless steels and aluminized type coatings exposed in in-situ oil shale retorting environments is being investigated. To date 11 simulated in-situ retorts and 2 underground retorts have been utilized to test 12 different steel alloy compositions and one steel coating material. The alloys have been exposed in these retorts to temperatures up to 1000°C for time periods up to 80 hours. Both Antrim and Green River type shales were being retorted at the time of the metal sample tests. The specimens were exposed directly in the shale beds near the location of monitoring thermocouple wells. To date, 160 specimens have been tested.

1. CORROSION IN SIMULATED IN-SITU OIL SHALE RETORTS

A. Levy and E. Elliott

It has been determined that different alloys corrode in different manners and to different degrees in high sulfur (3.2%) antrim shale and in low sulfur (0.8%) Green River Shale. In tests with antrim shale in the LETC 10 ton retort, 18% reduction in metal thickness occurred in 347 stainless steel exposed to temperatures above 1500°F for exposure times of only 40 hours. In general, the corrosion of 300 series stainless steels observed in Green River shale exposures is markedly less than that which occurs when antrim shale is retorted. Figure 1 shows this difference on 310SS. Note the magnification difference in the two photos. However, the lower chromium content 410 stainless steel corroded more than 347SS in the low sulfur Green River shale. It corroded less than 347SS in antrim shale. The morphology of the scale products and their chemical composition differed from alloy to alloy in antrim shale.

The higher chromium content alloys formed some Cr_2O_3 as well as considerable iron and chromium sulfides and iron-chrome sulfide spinels in layers while the lower chromium content alloys only formed sulfides. Non-chromium containing alloys underwent extensive sulfidation. In Green River shale, the 300 series stainless steels only formed a protective Cr_2O_3 scale layer and no sulfides. Generally, the Green River shale retort specimens were exposed to lower temperatures and times than the antrim shale retort specimens as well as to a lower sulfur content shale.

A marked difference in the corrosive attack also occurred as the result of exposures to large and smaller oil content shales. Figure 2 shows

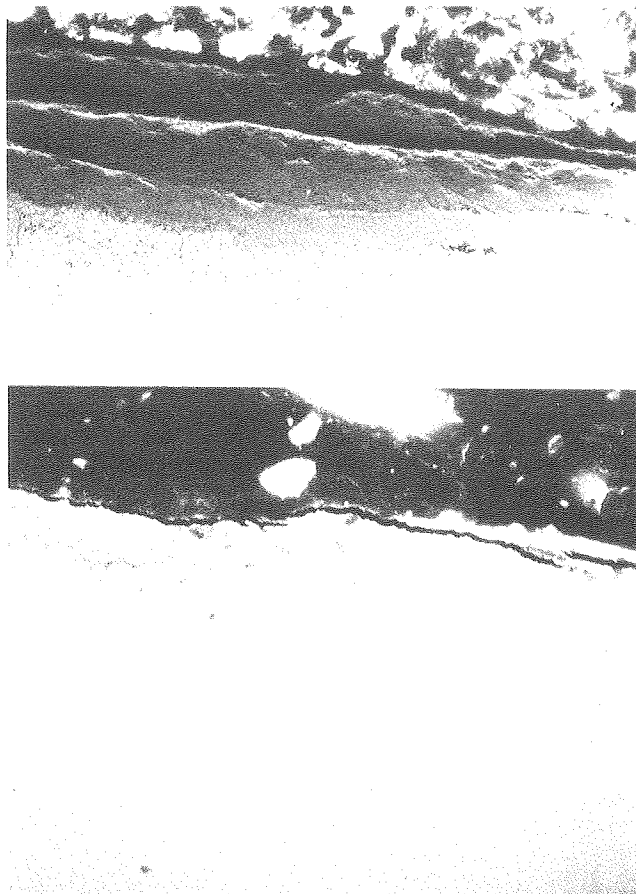


Fig. 1. Scales formed on 310SS exposed in simulated antrim (above, 200X) and Green River (below, 3000X) shale retorting operations. (XBB 7912-16283)

specimens of 410SS exposed to a high (36 gal/ton) Green River shale (upper photo) and a lower (18 gal/ton) shale in the same simulated in-situ retort run at LLL. The samples exposed to the richer shale were more heavily attacked and had a porous, single phase scale. A thinner, dense, two phase scale formed on the specimens in the leaner shale.

Aluminide coatings formed a protective Al_2O_3 scale on both stainless and low alloy steels and protected them from attack under all of the retort conditions and types of shale tested. See Fig. 3 for 1018 mild steel. The underground tests conducted were not productive in establishing corrosion behavior patterns because of lack of control in their placement and difficulty in their recovery.

* * *

* This work was supported by the Division of Planning and Systems Engineering, Office of Fossil Energy, U. S. Department of Energy.

† Brief version of LBL-9906; to be presented at NACE Corrosion 80, Chicago, IL, March 1980.

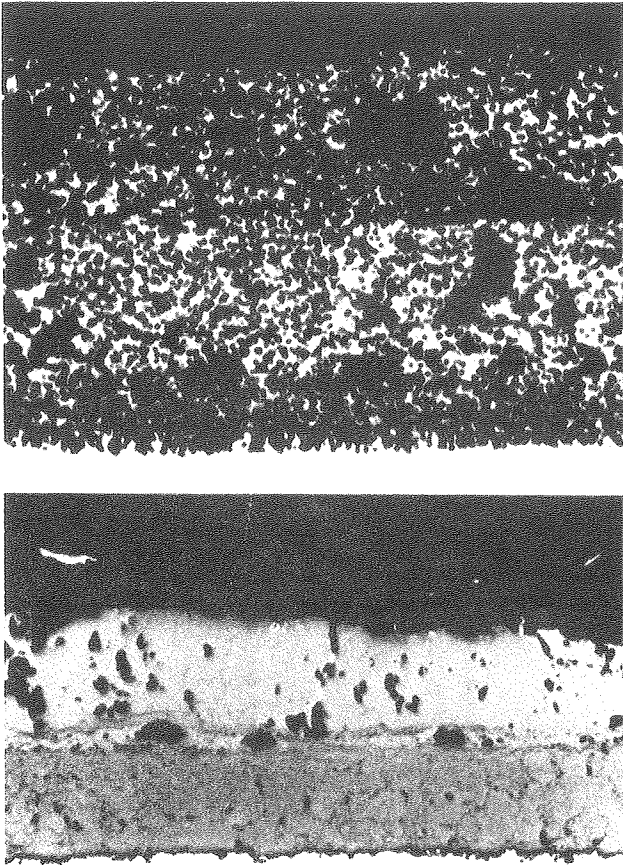


Fig. 2. Scales formed on 410SS exposed in rich Green River Shale (above, 200X) and lean Green River Shale (below, 400X). (XBB 7912-16284)

RESEARCH PLANS FOR CALENDAR YEAR 1980

Sufficient knowledge has been obtained from specimen exposures in simulated in-situ retorts to develop a test program where specimens will primarily be exposed in laboratory crucible tests using Green River and antrim shales with bulk gas compositions over the shales that simulate retort conditions. More controlled temperatures and times representative of the higher temperature, longer time exposures that will occur in underground retorting operations can be achieved in the crucible tests.

Additional coating tests will be conducted on low alloy and stainless steels with the objective of finding the lowest possible cost combination of coating and alloy that can withstand underground retorting environments. Specimens, coated and

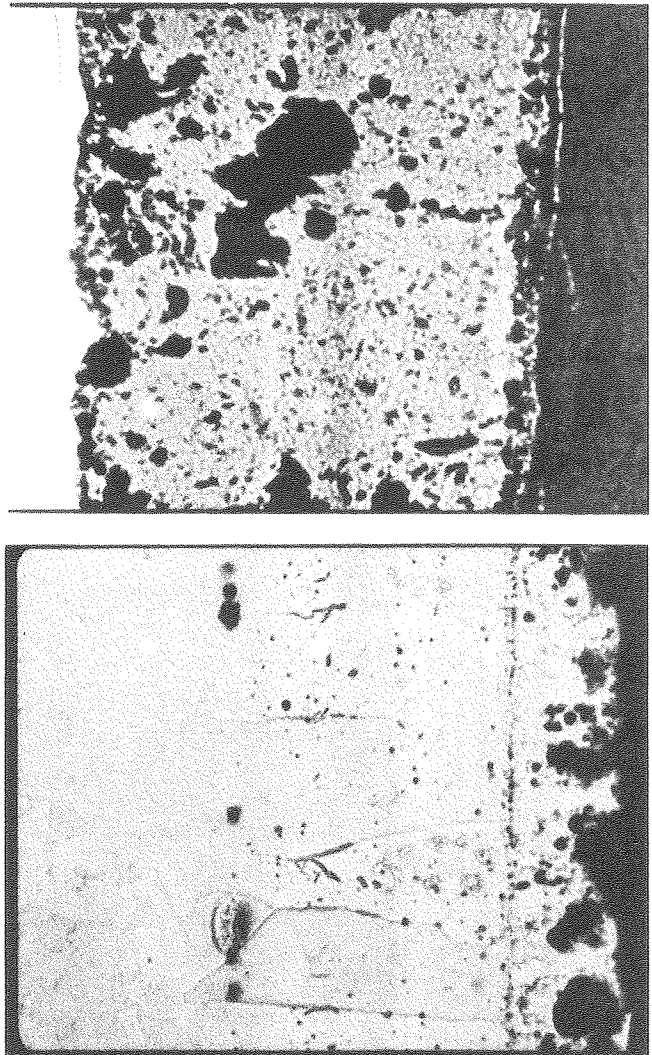


Fig. 3. Scales formed on 1018 mild steel without coating (above, 320X) and with coating (below, 320X). (XBB 7912-16285)

uncoated, will be placed in underground retort tests as they become available. Tests will also be conducted in shale oil product material.

1979 PUBLICATIONS AND REPORTS

Invited Talk

1. A. V. Levy, "Corrosion of Metals in Oil Shale Retorts," ASM WESTEC '79, Los Angeles, Calif., March, 1979.

